A Computational Study of the Raman Spectra of Large Polycyclic Aromatic Hydrocarbons: Toward Molecularly Defined Subunits of Graphite†

Fabrizia Negri,*,‡ Chiara Castiglioni,*,§ Matteo Tommasini,§ and Giuseppe Zerbi§

Dipartimento di Chimica "G. Ciamician", Università di Bologna, 40126 Bologna, Italy, and Dipartimento di Chimica Industriale e Ingegneria Chimica, Politecnico di Milano, Piazza Leonardo da Vinci 32, 20133 Milano, Italy

Received: July 24, 2001

We present a quantum chemical investigation of the vibrational frequencies and Raman intensities of large polycyclic aromatic hydrocarbons (PAHs) as models for nanosized graphitic domains in carbon materials. The gradient corrected BLYP functional, in the framework of density functional theory, was employed to compute equilibrium structures, vibrational force fields, and Raman intensities. Molecules of different size (from 24 to 138 carbon atoms) and symmetry (D_{6h}, D_{3h}, D_{2h}) were investigated. It is shown that the simulated Raman spectra compare well with the available experimental spectra. The analysis of Raman activities in terms of local contributions from internal coordinates shows that the PAHs can be grouped in essentially two classes related more strictly to their "benzenoid" character than to the shape of their periphery. The analysis of local contributions to polarizability derivatives combined with the shape of the molecular motion of the Raman active vibrations in the 1300 cm^{-1} region of PAHs supports the mechanism recently proposed by us to explain the appearance of the D band in disordered graphitic materials.

1. Introduction

Polycyclic aromatic hydrocarbons (PAHs) have attracted the interest of the scientific community since long ago, for several different reasons. From a theoretical point of view they represent a class of compounds extensively investigated to test elementary π-bond theories.[1] On the other hand, some PAHs are studied for their carcinogenic activities,[2] for their possible presence in the interstellar media,[3] and for their self-organizing properties.[4]

Until recently, however, the number of PAHs isolated and/or synthesized was relatively small and limited to small sizes.[5] Very recently a new synthetic route has been developed[6] and PAHs of very large size have become available. These large polycyclic aromatic hydrocarbons can be considered as molecularly defined graphite subunits, such as those present in defected graphite samples and other carbon materials. The availability of very large PAHs widens the range of potential applications of these conjugated systems. At the same time these molecularly defined objects can be investigated in order to provide explanations for some not yet well understood experimental behaviors observed for disordered carbon materials containing nanosize sp^2 structures.

A powerful tool widely employed to characterize the structure of materials is Raman spectroscopy. The Raman spectra of carbonaceous materials containing a variable amount of sp^2 structures have been extensively studied,[7] and it is well known that they contain two main signatures: first, a band located around 1580 cm^{-1}, which is known as the graphitic (G) band, since it is the only feature observed in the first order Raman spectrum of highly ordered, crystalline graphite. The second band appears at about 1350 cm^{-1} for disordered samples of graphite or in amorphous carbon materials containing sp^2 graphitic islands. It is known as the D band since it appears in connection with a variable amount of disorder or defects in the sample. Despite the fact that these two main signatures have been known for a long time, the mechanism lying behind the activation of the D band is not yet completely understood, along with several experimental data such as the dispersion of the D band with excitation wavelength[8] and the frequency shift in the anti-Stokes Raman spectra compared to the Stokes Raman spectra.[9]

Interestingly, the Raman spectra of PAHs are also characterized by few bands in approximately the same G and D regions. This is expected, given the similarity of their structure with graphitic islands, and offers the advantage of using molecules with a well-known dimension and structure to probe defects of similar size and structure in carbonaceous materials.

In previous works[10−14] we delineated the basis for a molecular approach to the interpretation of the Raman spectra of disordered graphitic materials. To this end we combined an experimental study of the Raman spectra of molecularly defined PAHs with a computational study of vibrational dynamics.[10,11] We extended the valence force field of Ohno[15] to infinite systems in order to describe the vibrational dynamics of graphite, and we compared the vibrational normal modes of selected PAHs with those of graphite.[11] From this study we concluded that a clear correlation exists between the D and G bands observed in disordered graphite samples and the Raman spectra of PAHs. In particular, it was shown that the shape of those vibrational modes of PAHs whose frequencies occur in the region of intense Raman bands resemble very closely the shape of the two phonons of graphite, which we labeled $\mathcal{A}$ and $\mathcal{A}$, respectively. The former is the only Raman active E_{2g} mode in a perfect graphite sheet, while the latter is the totally symmetric mode at the K point of the Brillouin zone.[11] The conclusion above, however, was reached

† Part of the special issue "Mitsuo Tasumi Festschrift".

* Corresponding authors. E-mail: fabry@ciam.unibo.it, chiara.castiglioni@polimi.it.

‡ Università di Bologna.

§ Politecnico di Milano.

10.1021/jp0128473 CCC: $22.00
Published on Web 01/22/2002

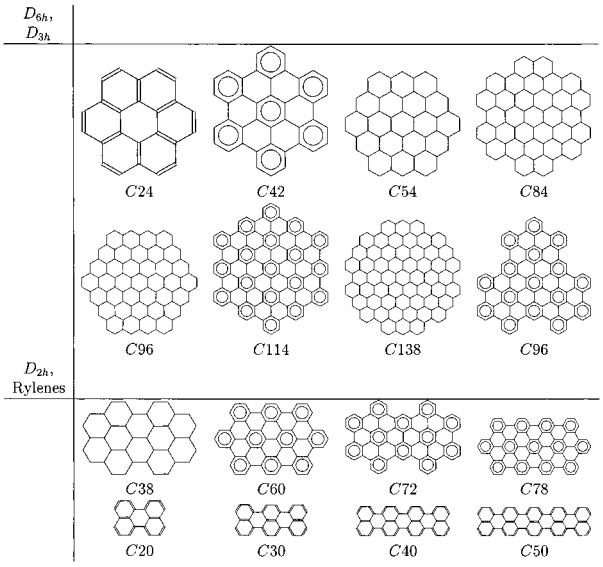

Figure 1. Molecular structure of the PAHs studied in this work.

by simply comparing the numerical values of the vibrational frequencies computed with the MO/8 force field for some PAHs, with the observed Raman bands. In other words, computational information on Raman intensities was missing at this level. To assess more quantitatively the connection between the Raman bands of graphite and Raman active modes of PAHs, we carried out a quantum-chemical study of vibrational force fields and Raman intensities on small PAHs (coronene and hexabenzocoronene) and confirmed that the strongest Raman active vibrational modes of PAHs are characterized by eigenvectors that show a large overlap with the two above-mentioned phonons of graphite.[12] In support of the evidence from the preliminary quantum-chemical calculations of ref 12, we recently discussed a simple model that accounts for the activation in Raman of the $\mathcal{A}$ phonon of graphite when a minimal rearrangement of the atomic and electronic structure occurs.[14] Obviously enough, an extension of quantum-chemical calculations to larger PAHs is required in order to confirm the conclusions drawn in our previous work and to gain more insight on the effect of shape and size of the confined sp^2 structure on Raman intensities. Thus, the objective of this work is two-fold: first we validate the theoretical approach employed previously for small PAHs by comparing computed and observed Raman spectra for a much larger and diverse sample of PAHs. Second, we demonstrate the efficiency of the present molecular approach to unravel the nature of the D band of graphitic materials by analyzing the computed polarizability derivatives in terms of local internal coordinate contributions.

2. Computational Details

The quantum-chemical calculations were carried out at the BLYP level of theory, a pure density functional theory (DFT) method that uses the Becke exchange functional[16] and the Lee, Yang, and Parr correlation functional.[17] The standard 6-31G basis set, as contained in the Gaussian 98 suite of programs,[18] was employed to obtain equilibrium structures, vibrational force fields, and Raman intensities.

The PAHs investigated in this work, characterized by different symmetry, shape, and size, are shown in Figure 1. They can be grouped into four different series: D_{6h} PAHs, D_{3h} PAHs, and D_{2h} PAHs that we label "2-dimensional", as opposed to the fourth group of highly anisotropic, "quasi 1-dimensional" D_{2h} PAHs (rylenes).

The analysis of local contributions to Raman intensities was carried out according to the following procedure.[19] From the polarizability derivatives with respect to the Cartesian nuclear displacements ($\partial\alpha/\partial x_i$), directly obtained from DFT calculations, the variations of the Raman polarizability tensors with respect to internal valence coordinates ($\partial\alpha/\partial R_t$) were calculated. The in-plane internal coordinates of each PAH can be divided into four subsets (CC stretchings, CH stretchings, CCC bendings, and CCH bendings). The following relationship,

$$\partial\alpha/\partial Q_j = \sum_t (\partial\alpha/\partial R_t) L_{tj} \qquad (1)$$

where L_{tj} is an element of the eigenvector describing the normal mode Q_j in terms of internal coordinates, allows to obtain Raman intensities as due to selected localized contributions. Indeed, if the sum in eq 1 is extended to all the internal degrees of freedom R_t, we exactly obtain the total DFT Raman intensities for the normal mode Q_j. On the other hand, if the sum is restricted just to some selected R_t coordinates, we can evaluate partial contributions to Raman intensities due to the subset considered. This analysis provides a useful tool to understand the intensity behavior of the main Raman lines along series of PAHs. In particular, since the polarizability derivatives associated with the stretching of CC bonds, $\partial\alpha/\partial R_{CC}$, show much larger values than any other local polarizability derivative, it will be particularly interesting to identify normal modes whose Raman intensity is dominated by CC stretching contributions. These contributions are collected in Tables 1−4 and will be thoroughly discussed in sections 3.2 and 3.3.

3. Results

3.1. Molecular Structure of PAHs. From Figure 1 it is seen that the PAHs investigated in this work can be grouped also according to their periphery, not just according to the symmetry group to which they belong. It is known that the electronic structure of large PAHs (and hence the molecular structure) depends not just on the size of the molecule but it is also related to the shape of its periphery.[20] The benzenoid character of PAHs is also related to the shape of the periphery. For PAHs made of six-membered carbon rings, the benzene-like behavior can be described in terms of Clar's aromatic sextets,[1] which are easily represented by drawing Robinson rings[21] inside carbon rings that contain aromatic sextets. The so-called "all-benzenoid" aromatic hydrocarbons are characterized by just one Clar formula, and the aromatic character takes over the olefinic character. Among the PAHs depicted in Figure 1, it can be seen that two of the D_{6h}, three of the D_{2h}, and the D_{3h} molecule belong to the class of all-benzenoid PAHs.

The all-benzenoid character must obviously be reflected, in some measure, on the structure of the ground state of PAHs. In other words, we expect to observe some common trend in the optimized geometries of the PAHs of similar nature. To summarize the information extracted from quantum-chemical calculations, we have numbered the CC bond lengths in D_{6h} PAHs from the center to the periphery in Figure 2, and we have plotted the CC bond lengths of the D_{6h} PAHs against the CC bond number in Figure 3a. The trend in the CC bond lengths is characterized by two regions: (i) the region close to the center of the D_{6h} PAH and (ii) the periphery. CC bond lengths take up a more distinct alternation pattern in the periphery of the PAH, while they show considerably less extensive alternation at the center of the PAH. Although BLYP/6-31G geometries appear to equalize considerably the CC bond lengths, especially at the center of the molecule, we can approximately group the

TABLE 1: PAHs of D_{6h} Point Symmetry: BLYP/6-31G Computed Raman Frequencies (cm^{-1}) and Intensities I_R ($Å^4$/amu)[a]

ν	I_R	I_R(CC)[b]	ν	I_R	I_R(CC)[b]	ν	I_R	I_R(CC)[b]	ν	I_R	I_R(CC)[b]
$C_{24}H_{12}$: A_{1g} modes			$C_{54}H_{18}$: A_{1g} modes			$C_{96}H_{24}$: A_{1g} modes			$C_{138}H_{30}$: A_{1g} modes		
472	115	103	321	222	212	243	373	374	1230	2154	2483
1030	26	50	818	147	206	1187	641	720	1283	64727	67906
1235	88	68	1213	73	75	1233	3476	3659	1307	10793	9710
1357	992	939	1286	3075	3362	1284	668	996	1321	35406	32705
1594	195	190	1340	4918	4320	1322	34142	31950	1371	4181	2946
			1405	453	472	1373	703	792	1396	1854	1760
			1461	1355	924	1406	1297	585	1423	1642	1367
			1616	1412	1437	1453	4729	3968	1471	1017	1211
						1552	1645	929	1501	1399	1048
						1611	6699	6419	1604	19146	16777
$C_{24}H_{12}$: E_{2g} modes			$C_{54}H_{18}$: E_{2g} modes			$C_{96}H_{24}$: E_{2g} modes			$C_{138}H_{30}$: E_{2g} modes		
296	18	0	251	73	0	1504	1412	967	1294	1000	737
366	37	0	1397	128	17	1564	1853	17	1318	891	624
660	23	0	1487	62	73	1574	3775	542	1346	1560	993
845	18	0	1545	584	56	1585	1862	22	1535	3525	117
991	17	3	1573	62	21	1604	542	146	1575	16558	781
1241	28	6	1592	1855	23				1618	1105	1142
1400	12	0									
1457	42	0									
1600	384	1									
$C_{42}H_{18}$: A_{1g} modes			$C_{84}H_{24}$: A_{1g} modes			$C_{114}H_{30}$: A_{1g} modes					
341	136	114	253	315	291	1098	730	1016			
1002	122	111	1253	1890	1862	1292	51128	46400			
1156	154	512	1301	380	175	1312	23775	23136			
1299	4823	3999	1325	28316	27331	1325	3107	3227			
1347	642	466	1371	1668	1628	1358	2234	1881			
1393	116	143	1608	2024	1914	1591	595	837			
						1602	1230	669			
$C_{42}H_{18}$: E_{2g} modes			$C_{84}H_{24}$: E_{2g} modes			$C_{114}H_{30}$: E_{2g} modes					
836	79	40	1370	470	403	1276	1410	958			
1259	128	42	1504	1257	166	1324	1579	946			
1290	148	72	1542	1022	58	1507	630	35			
1349	176	77	1584	5169	220	1531	2935	301			
1453	344	123	1610	374	293	1568	8603	467			
1534	248	52				1577	1457	3			
1572	987	12									
1590	667	9									

[a] Only vibrations whose Raman intensity is larger than 1/100 I_{max}(I_{max} = Raman intensity of the strongest transition of the molecule considered) are reported. CH stretchings are not included. [b] Contribution from CC stretchings, computed using eq 1 where only derivatives with respect to $R_t = R_{CC}$ are included.

TABLE 2: PAH of D_{3h} Point Symmetry: BLYP/6-31G Computed Raman Frequencies (cm^{-1}) and Intensities I_R ($Å^4$/amu)[a]

	$C_{96}H_{30}$		
	ν	I_R	I_R(CC)[b]
A_1' modes	1306	48416	44615
	1310	1374	866
	1337	1802	1745
	1383	2771	2063
	1571	713	180
E_1' modes	1308	1806	1490
	1311	1403	1060
	1507	883	238
	1539	1326	332
	1571	9216	880
	1589	1148	224
	1590	555	6
	1594	638	246

[a] Only vibrations whose Raman intensity is larger than 1/100 I_{max}(I_{max} = Raman intensity of the strongest transition of the molecule considered) are reported. CH stretchings are not included. [b] Contribution from CC stretchings, computed using eq 1 where only derivatives with respect to $R_t = R_{CC}$ are included.

PAHs studied in two classes according to the structure of the core of the molecule (bonds in the range 1−5 of Figure 3a). The all-benzenoid PAHs C42 and C114 and the partially benzenoid C54 belong to the first group. (To simplify the notation in the following we will call each planar PAH by the symbol CX, where X is the number of carbon atoms, omitting the number of hydrogen atoms. When ambiguity is possible, as for C96 (D_{3h}) and C96 (D_{6h}), we explicitly indicate also the symmetry group of the molecule.) C84 and C96, partially benzenoid PAHs, belong to the second group. C24, the smallest member among the D_{6h} systems considered here, contains only three different CC bonds, one of which is a short peripheral bond. Thus it is difficult to include it in one of the two above classes. C138, the largest D_{6h} PAH considered, shows CC bonds much more equalized than the other PAHs, although the trend follows that of all-benzenoid PAHs. A marked equalization can be connected with its only partially benzenoid nature and with its larger dimension. Generally speaking, we can conclude that all-benzenoid PAHs have bond 1 (see Figure 2) shorter than bond 2, while the opposite is true for markedly nonbenzenoid PAHs such as C84 and C96.

Concerning the molecular structures, it is interesting to compare the structure of all-benzenoid PAHs across symmetry groups. C114 (D_{6h}) and C78 (D_{2h}) are both all-benzenoid PAHs, but they belong to different symmetries. However, we can see from Figure 2 that C78 can be thought as C114 without two terrylene units on both sides of the molecule. Thus we can adopt for C78 the same CC bond numbering employed for C114 and compare the bond lengths that correspond to the same numbering in the two structures. This is done in Figure 3b. Obviously,

TABLE 3: PAHs of D_{2h} Point Symmetry: BLYP/6-31G Computed Raman Frequencies (cm^{-1}) and Intensities I_R ($Å^4$/amu)[a]

	$C_{38}H_{16}$			$C_{60}H_{22}$			$C_{72}H_{26}$			$C_{78}H_{26}$		
	ν	I_R	I_R(CC)[b]	ν	I_R	I_R(CC)[b]	ν	I_R	I_R(CC)[b]	ν	I_R	I_R(CC)[b]
A_g modes	272	74	24	323	171	173	1250	336	371	317	372	413
	440	89	107	1073	243	262	1270	405	266	1261	326	499
	1224	65	29	1154	106	567	1304	26498	24212	1276	21035	19664
	1237	118	143	1281	3101	2798	1326	355	281	1293	18049	16058
	1258	301	264	1296	9417	8198	1339	4461	3515	1313	5263	4556
	1322	311	202	1323	3083	2591	1350	2308	1679	1320	1693	1460
	1342	4341	3841	1344	267	316	1391	766	668	1339	4877	4893
	1372	459	580	1349	892	772	1494	1220	705	1346	1628	1221
	1436	88	46	1364	121	70	1538	1197	605	1360	488	408
	1457	107	28	1387	279	224	1573	3241	524	1371	332	286
	1521	55	43	1464	762	370	1589	1192	222	1471	2858	2013
	1591	310	242	1520	1045	507				1513	4102	2669
	1608	513	327	1572	4872	2191				1572	27345	19639
				1593	840	338				1593	8540	5680
				1601	843	497				1595	559	707
B_{3g} modes	1462	75	18	1267	185	135	1311	708	472	1269	536	458
	1478	56	2	1284	267	186	1464	1008	489	1283	457	332
	1589	512	16	1333	488	323	1536	538	172	1328	1305	921
	1607	156	19	1574	402	179	1570	3692	917			
							1588	1279	279			
							1592	611	459			

[a] Only vibrations whose Raman intensity is larger than 1/100 I_{max}(I_{max} = Raman intensity of the strongest transition of the molecule considered) are reported. CH stretchings are not included. [b] Contribution from CC stretchings, computed using eq 1 where only derivatives with respect to $R_t = R_{CC}$ are included.

TABLE 4: Rylenes (D_{2h} Point Symmetry): BLYP/6-31G Computed Raman Frequencies (cm^{-1}) and Intensities I_R ($Å^4$/Amu)[a]

	perylene			terrylene			quaterrylene			pentarylene		
	ν	I_R	I_R(CC)[b]	ν	I_R	I_R(CC)[b]	ν	I_R	I_R(CC)[b]	ν	I_R	I_R(CC)[b]
A_g modes	544	93	95	535	396	423	548	1569	1727	537	5680	5627
	975	141	125	1035	798	814	1062	2981	3259	1078	8039	9021
	1111	53	91	1229	578	710	1232	3764	4537	1229	15162	17310
	1315	1165	916	1285	8300	7259	1267	53584	50262	1254	228359	219640
	1365	177	247	1316	8003	7194	1305	36170	32667	1300	69387	61449
	1370	399	474	1357	256	365	1368	9726	11586	1319	3802	3178
	1457	56	38	1367	2947	3562	1533	86755	87136	1365	4323	4808
	1552	2441	1832	1541	21119	19600				1371	8789	9829
	1591	66	38	1585	730	656				1372	10746	12986
										1525	234232	244675
B_{3g} modes	363	39	5	1240	222	146	1598	1077	2973			
	1169	59	33	1600	520	1817						
	1244	81	45									
	1467	37	25									
	1607	84	590									

[a] Only vibrations whose Raman intensity is larger than 1/100 I_{max}(I_{max} = Raman intensity of the strongest transition of the molecule considered) are reported. CH stretchings are not included. [b] Contribution from CC stretchings, computed using eq 1 where only derivatives with respect to $R_t = R_{CC}$ are included.

owing to its lower symmetry, bonds that are equivalent in C114 are no longer so in C78. Thus, for instance, there are two choices for CC bond number 1, two for CC number 2, three for CC number 3, and so on. In Figure 3b we report the bond lengths that correspond to only one of such possible choices, which is depicted in Figure 2 (bottom, right). We made this choice since the numbering in Figure 2 (bottom, right) flows on the internal part of C78, that we expect to be less perturbed and more appropriate for comparison with C114. Nevertheless, a very similar graph would be obtained by using an alternative choice of equivalent CC bonds for C78. The similarity between CC bond lengths in the two structures is impressive and provides additional support to the idea that the bond lengths in all-benzenoid structures follow very similar trends also when going across symmetry groups to which the PAHs belong. In section 3.3 it will be seen that this behavior is even more strongly apparent when looking at the electronic properties such as the polarizability derivatives (Figures 3c, 3d).

3.2. Computed and Observed Raman Spectra of Large PAHs. The Raman spectra computed for the PAHs considered in this work are presented in Figure 4. The computed spectra are compared with the experimental spectra for all the PAHs for which the latter are available,[10] namely for the all-benzenoid structures C42, C114, C96 (D_{3h}), C60, C72 and C78 and for coronene. These spectra were recorded on solid samples using the following excitation laser wavelengths: 1064 nm for coronene and C42; 632.8 nm for all the other PAHs. In addition to 2D-PAHs, experimental spectra are also available for the class of rylenes, which can be considered quasi 1D-PAHs. In this case the experimental spectra were recorded for *tert*-butyl substituted rylenes[22] with excitation at 1064 nm. It will be seen, however, that substituents have little effect on the spectra that can be very well analyzed in terms of the calculations carried out on unsubstituted PAHs.

Owing to the size of most of the PAHs considered in this work, the number of vibrational frequencies is often very large. For this reason, in Tables 1−4 we collected only the vibrational

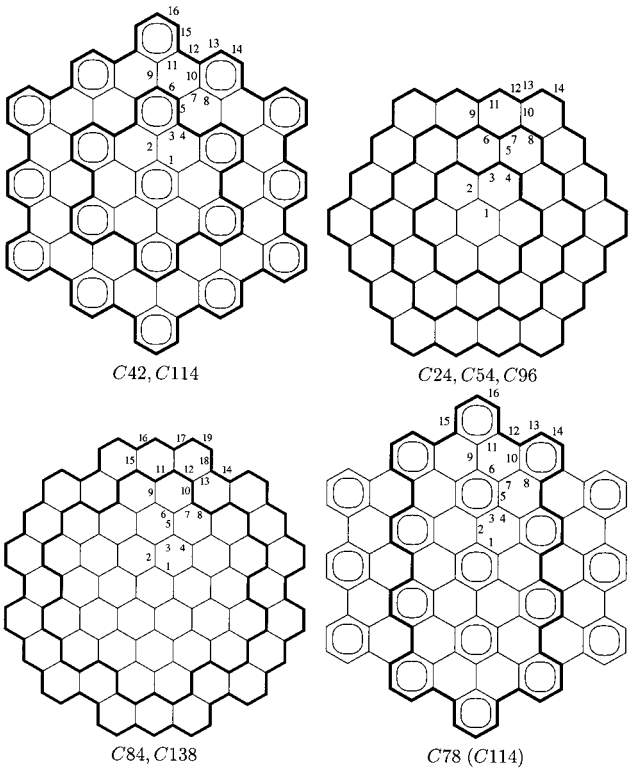

Figure 2. Numbering of carbon−carbon bonds for D_{6h} PAHs and for C78 (D_{2h}).

frequencies associated with the strongest computed Raman activity, that is only vibrations whose Raman intensity is computed to be 1/100 I_{max} (I_{max} = strongest Raman intensity for each molecule). Inspection of Tables 1−4 indicates that only few vibrations are indeed Raman active, out of all the vibrations Raman active for symmetry reasons. Furthermore, most of the Raman activity is concentrated around 1300 and 1600 cm^{-1}, in agreement with the available experimental spectra. Indeed, a cursory comparison between computed and observed Raman spectra in Figure 4a and 4c shows an overall satisfactory agreement.

Moving to a more detailed analysis of the spectra depicted in Figure 4a, we assign the frequency computed at 1600 cm^{-1} (BLYP/6-31G) for C24 to the band observed at 1627 cm^{-1}. The simulated band at 1600 cm^{-1} contains a contribution from a second fundamental, of A_{1g} symmetry, computed at 1594 cm^{-1}. This frequency can be assigned to the observed 1584 cm^{-1} band. In the 1300 cm^{-1} region two bands are observed at 1349 and 1366 cm^{-1}, while only one strong band is computed at 1357 cm^{-1}. However, previous calculations[23] and experimental studies[24] of the Raman spectra of coronene showed that the observed doublet is due to a Fermi resonance.

Concerning C42, we can readily assign the computed 1299 and 1347 cm^{-1} frequencies to the bands observed at 1313 and 1365 cm^{-1}, respectively. The intensity of the latter band is underestimated by BLYP/6-31G calculations, probably because of an imperfect mixing of local coordinates in the two normal modes. In the higher frequency region, two bands are observed at 1596 and 1613 cm^{-1}and correspondingly two bands are computed at 1572 and 1590 cm^{-1}. A tendency to underestimate the vibrational frequencies in the 1600 cm^{-1} region is already found for C24 and appears to be characteristic of the BLYP/6-31G level of theory.

The experimental spectrum recorded for C114 shows a single band at 1604 cm^{-1} and a prominent band at 1319 cm^{-1} followed by a weaker band at 1282 cm^{-1}. We assign the first band to the computed 1568 cm^{-1} fundamental. The calculations predict two bands at 1312 and 1292 cm^{-1} that can be assigned to the 1319 and 1282 cm^{-1} experimental bands, although the computed intensities appear to be reversed as compared to the observed ones. Again, this is probably due to the imperfect mixing, at the BLYP/6-31G level, of local contributions (CC stretching, CH wagging) in the two normal modes. Given the large number of normal modes in a narrow frequency region, this unbalanced mixing is not surprising. The weak feature observed at 1365 cm^{-1} is also accounted for by the computed 1358 cm^{-1} band.

The experimental spectrum of C96(D_{3h}) shows two prominent bands at 1604 and 1320 cm^{-1} and a weaker feature at ca. 1250 cm^{-1}. The two main bands are readily assigned to the computed 1571 and 1306 cm^{-1} fundamentals, although we notice an underestimate of both the intensity and the frequency of the former band. As noted before, the frequency underestimate is computed for all the PAHs so far considered. Concerning the intensity underestimate, we cannot rule out resonance effects in the experimental spectrum. These were not included in the present calculations.

The experimental spectra of 2D D_{2h} PAHs, shown on the top part of Figure 4a, are characterized by a prominent band at about 1600 cm^{-1} and a couple of bands around ca. 1330 and 1260 cm^{-1}. The calculations account well for the prominent feature in the high-frequency region, although the computed frequency is underestimated (1572 cm^{-1} computed versus 1601 cm^{-1} observed for C60; 1573 cm^{-1} computed versus 1603 cm^{-1} observed for C72; 1572 cm^{-1} computed versus 1597 cm^{-1} observed for C78). In agreement with the observed spectra, two main bands are computed in the 1300 cm^{-1} frequency region, although the frequency difference between them is smaller than the observed separation, and the intensity ratio is reversed with respect to the observed trend, except for C78. For instance, the two bands at 1339 and 1263 cm^{-1} observed for C72 are assigned to the computed 1339 and 1304 cm^{-1} fundamentals. Interestingly, the experimental spectrum of C78 is more structured than those of C60 and C72, and correspondingly a pronounced substructure is also computed. Consider for instance the bands observed at 1261 and 1236 cm^{-1} that are assigned to the 1293 cm^{-1} and 1276 cm^{-1} BLYP/6-31G fundamentals. On the higher frequency side, two additional bands are observed, at 1333 cm^{-1} and a shoulder at ca. 1313 cm^{-1}, and two bands are correspondingly computed at 1339 and 1313 cm^{-1}.

In Figure 4b we collected the computed Raman spectra for those PAHs whose experimental spectra are not available. It is interesting to note that the remarkably non-benzenoid PAHs C84 and C96 (see the discussion in section 3.1) show rather similar spectra (a single strong band in the 1300 cm^{-1} region). The same is true (similar Raman spectra, two bands in the 1300 cm^{-1} region) for the remaining two D_{6h} PAHs, C138 and C54. These are not all-benzenoid but, as discussed in Section 3.1, the trend in their CC bond lengths follows that of all-benzenoid PAHs. In other words, all the calculated properties (geometries, Raman spectra) seem to indicate a natural classification of the PAHs investigated here, in approximately two groups. The analysis in terms of local polarizability derivatives discussed in the next section will provide further support to this classification.

The quasi-1D shape of rylenes results in Raman spectra that show, experimentally, stronger intensity in the 1600 cm^{-1} region. This trend is nicely reproduced by the calculations, as can be seen from Figure 4c. The experimental spectrum of alkyl-

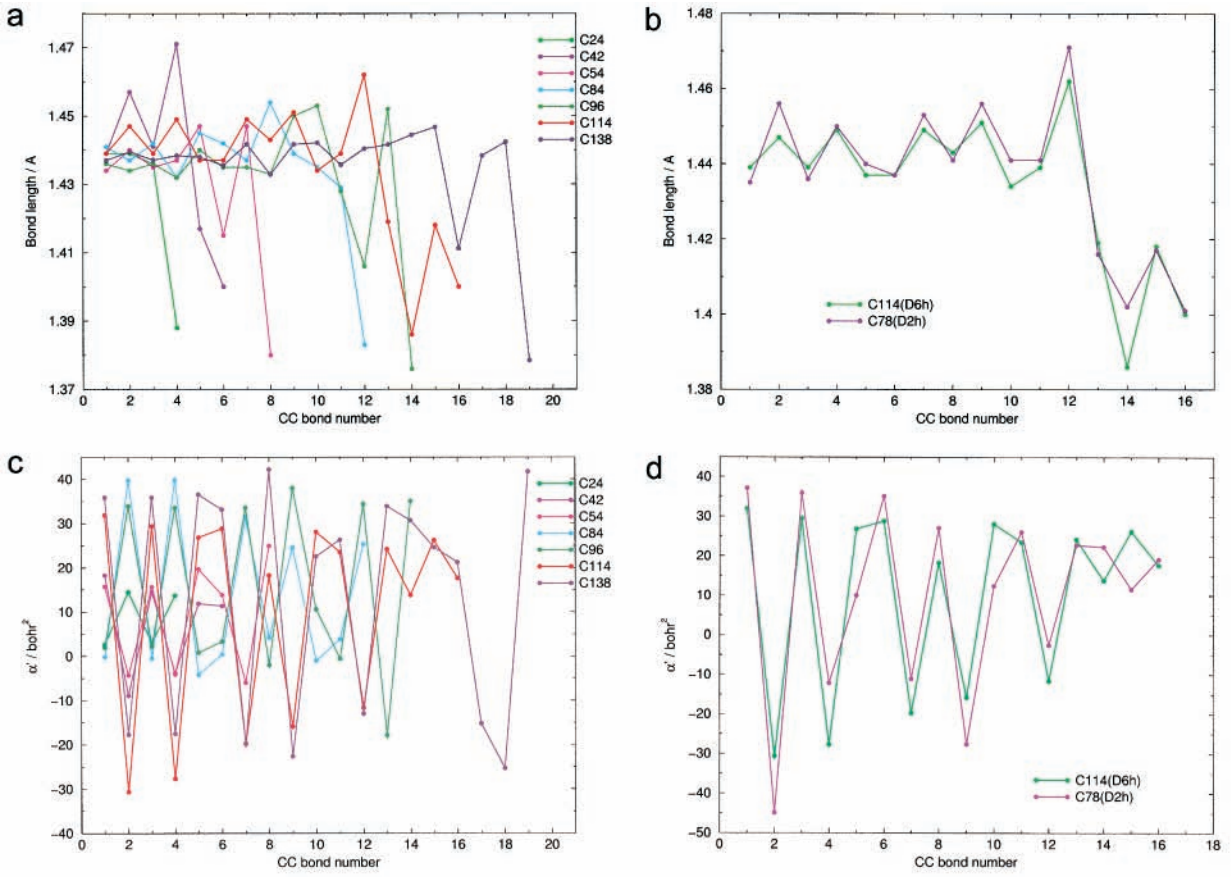

Figure 3. (a) Comparison of CC bond lengths in D_{6h} PAHs. (b) Comparison of CC bond lengths in C114 (D_{6h}) and C78 (D_{2h}). (c) Comparison of α' invariants in D_{6h} PAHs. (d) Comparison of α' invariants in C114 (D_{6h}) and C78 (D_{2h}).

substituted perylene shows three prominent bands at 1569, 1365, and 1296 cm^{-1}. These are nicely reproduced by the fundamentals computed at 1552, 1365, 1370, and 1315 cm^{-1}. In the observed spectrum there are additional weaker features at 1450, 1232, 1157, and 1010 cm^{-1} that are readily assigned to the fundamentals computed at 1457, 1244, 1170, and 975 cm^{-1}.

The Raman spectrum of alkyl-substituted terrylene is more structured in the 1300 cm^{-1} region: there is a single strong band at 1562 cm^{-1} followed by five bands at 1373, 1346, 1311, 1283, and 1246 cm^{-1}, and finally another band is observed at 1067 cm^{-1}. This pattern is very well reproduced by the simulated spectrum that shows a prominent band at 1541 cm^{-1} followed by four bands, the first of which is due to two fundamentals computed very close at 1367 and 1357 cm^{-1}. The three remaining bands are computed at 1316, 1285, and 1229 cm^{-1}. Finally, the fundamental computed at 1035 cm^{-1} is assigned to the observed 1067 cm^{-1} band. The computed intensity ratio is also very well predicted.

The Raman spectrum of quaterrylene shows, as for previous rylenes, a single band at 1550 cm^{-1} and a more structured region around 1300 cm^{-1} where four bands are observed at 1345 cm^{-1}, at ca. 1285 cm^{-1}, at 1264 cm^{-1}, and 1241 cm^{-1}. Another medium intensity band is observed at 1078 cm^{-1}. The calculations assign the highest frequency band to the computed 1533 cm^{-1} fundamental. In the 1300 cm^{-1} region there are four calculated bands at 1368, 1305, 1267, and 1232 cm^{-1} that can be assigned to the four observed bands, although the intensity ratio of the 1305 and 1232 cm^{-1} computed bands is reversed when compared to the experimental 1285 and 1241 cm^{-1} bands. The band observed at 1078 cm^{-1} is assigned to the fundamental computed at 1062 cm^{-1}.

The experimental Raman spectrum of pentarylene is simpler than the previous ones, since it shows two main bands at 1530 and 1230 cm^{-1}, two weak features at 1344 and 1084 cm^{-1}, and a shoulder on the higher frequency side of the 1230 cm^{-1} band. We assign the 1530 cm^{-1} band to the computed 1525 cm^{-1} fundamental, the 1230 cm^{-1} band to the computed 1254 cm^{-1} band, and the two weak features at 1344 and 1084 cm^{-1} to the 1371, 1372, and 1078 cm^{-1} computed fundamentals, respectively. The additional computed band at 1300 cm^{-1} is attributed to the aforementioned shoulder of the 1230 cm^{-1} observed band.

In summary, the computed Raman spectra are in good agreement with the observed spectra. The closest agreement is obtained for C24, C42, and for rylenes, that is for those PAHs for which the Raman spectrum was recorded out of resonance, at 1064 nm. For the other PAHs, the wavelength employed (632.8 nm) may fall in preresonance/resonance with some $\pi\pi^*$ electronic transition. In this case, resonance effects may be responsible for the less quantitative agreement between observed and computed spectra. Work in the direction of computing resonance Raman contributions is in progress.

Inspection of Figure 4 shows that most of the activity in Raman is observed and computed in the 1300 cm^{-1} region, that is the region of the D band of disordered carbon samples. The calculations show that the strong Raman activity in this region is associated with vibrations dominated by CC stretching motions. These CC oscillations combine in such a way that a breathing of selected carbon rings results, as is shown in Figure 5 where the shape of the vibrations associated with the strongest Raman intensity is depicted for all the PAHs studied in this work. In other words, the BLYP/6-31G calculations carried out on this large sample of PAHs indicate that the strongest Raman

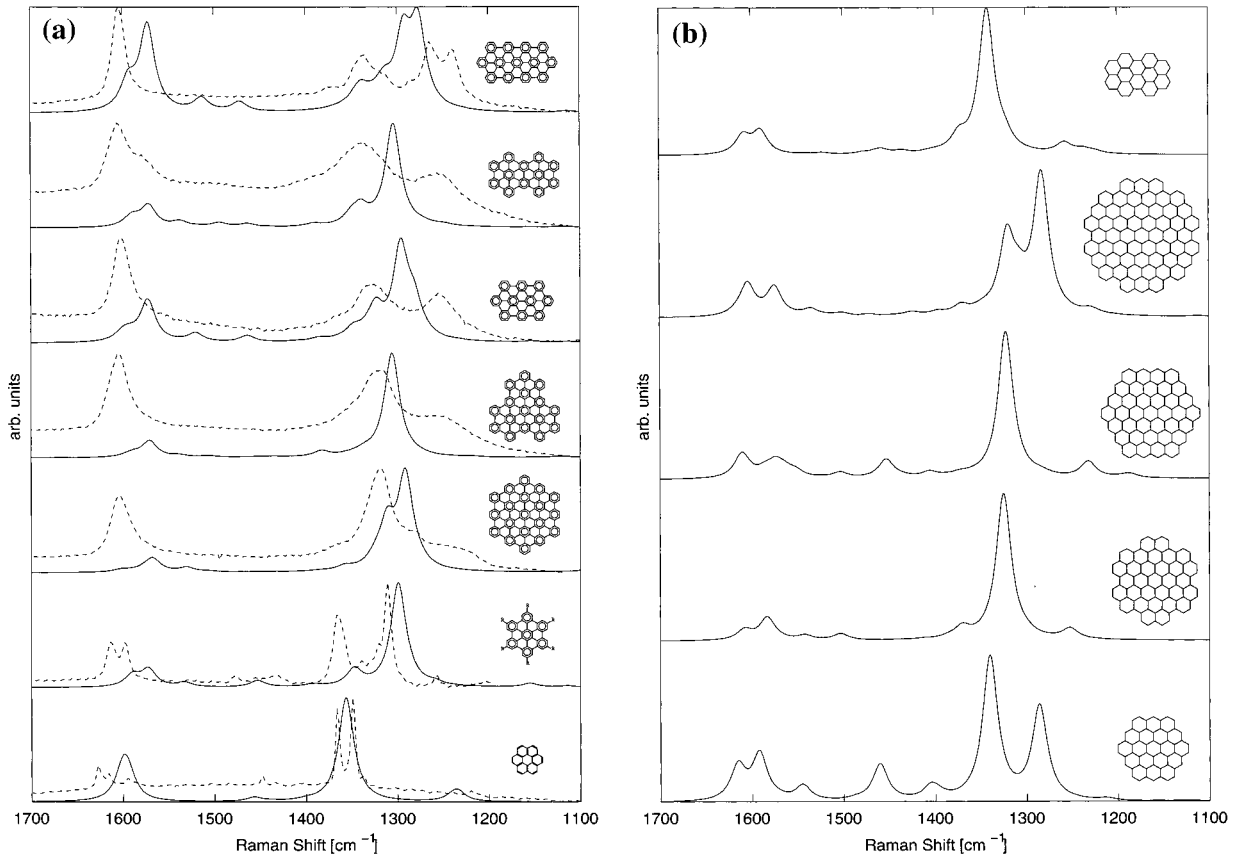

Figure 4. Calculated Raman spectra for the PAHs studied in this work and comparison (when available) with the corresponding experimental spectra. A Lorenzian line width of 20 cm^{-1} was employed to obtain simulated spectra more easily comparable with the experimental data. (a) Comparison between calculated (solid line) and observed (dashed line) spectra for D_{6h}, 2D-D_{2h}, and D_{3h} PAHs. (b) Calculated spectra for D_{6h} and 2D-D_{2h} for which experimental data are not available. (c) Comparison between calculated (bottom) and observed (top) spectra for 1D-D_{2h} (rylenes).

active vibrations in the region of the D band are characterized by a remarkable similarity with the $\mathcal{A}$ phonon of graphite.[11,14] We will come back to the relevance of this observation in the next sections.

Strictly related to the nature of the strong Raman modes is the magnitude of the local CC stretching contributions to Raman intensity. As anticipated in section 2, these local contributions are larger than any other local contribution. Inspection of the I_R(CC) data collected in Tables 1−4 shows that the modes strongly active in Raman in the 1300 cm^{-1} have the largest I_R(CC) contributions. Furthermore, these local contributions account almost completely for the total Raman intensity, as can be seen by comparing the numbers in the I_R(CC) columns with those in the I_R columns, for the strong Raman active modes in the 1300 cm^{-1} region.

3.3. Analysis of Computed Polarizability Derivatives in Terms of Local Contributions. The discussion of computed Raman intensity in PAHs reported in section 3.2, along with the inspection of Tables 1−4 and Figure 4, brings to the following remarks. (i) Generally speaking, within a given class of PAHs, the total Raman activity increases (more than linearly) when increasing the size of the molecule. Under this point of view a remarkably different behavior is observed for 2-dimensional (D_{6h}, D_{3h}, and D_{2h}) PAHs and for 1-dimensional PAHs (rylenes). This last series shows the largest intensity values, up to 2 orders of magnitude larger than those of 2-dimensional PAHs of comparable size. Compare, for instance, $I_{max} = 234232$ Å^4/amu for pentarylene (50 C atoms)[22] with $I_{max} = 4918$ Å^4/amu for circumcoronene (54 C atoms). (ii) For D_{6h}, D_{3h} PAHs the Raman spectra are dominated by bands in a region near 1300 cm^{-1}, associated with normal modes that belong to totally symmetric species. (iii) In the case of rylenes, two main features of comparable intensity are found (one band near 1550 cm^{-1} and a pair of bands near 1300 cm^{-1}). (iv) D_{2h} 2-dimensional systems show an intermediate behavior: the features near 1600 cm^{-1} become relatively more important, as the "anisotropy" of the system increases (compare for instance C78 with C72). (v) Inspection of the computed CC stretching contributions to Raman intensity (see Tables 1−4) always shows that the strongest Raman bands belonging to totally symmetric species are dominated by polarizability changes associated with the stretching of CC bonds.

Observation (v) suggests that the origin of the intensity behavior described from points (i) to (iv) can be rationalized by analyzing and comparing the local CC stretching parameters $\partial\alpha/\partial R_{CC}$, which enter the expression for Raman intensity (see eq 1). In Table 5 we report the values of CC stretching polarizability tensors for a selection of molecules. In Figures 3c and 3d the values of the invariant $\alpha' = 1/3\ \mathrm{Tr}(\partial\alpha/\partial R_{CC})$ are plotted against the CC bond number, for all the D_{6h} molecules and for C78.

The analysis of these data brings to the following statements. (1) The CC stretching polarizability tensors show larger values compared with the polarizability derivatives over the other internal coordinates: for instance the α' values of CC stretching tensors are 1 to 2 orders of magnitude larger than the α' values of CCC and CCH bending tensors. A direct consequence of this fact is point (v) above. (2) The class of rylenes shows anomalously large stretching polarizability tensors for the bonds along the molecular periphery. Their magnitude is clearly responsible for the huge Raman activity of some totally symmetric Raman bands (see points (i) and (iii)). (3) The

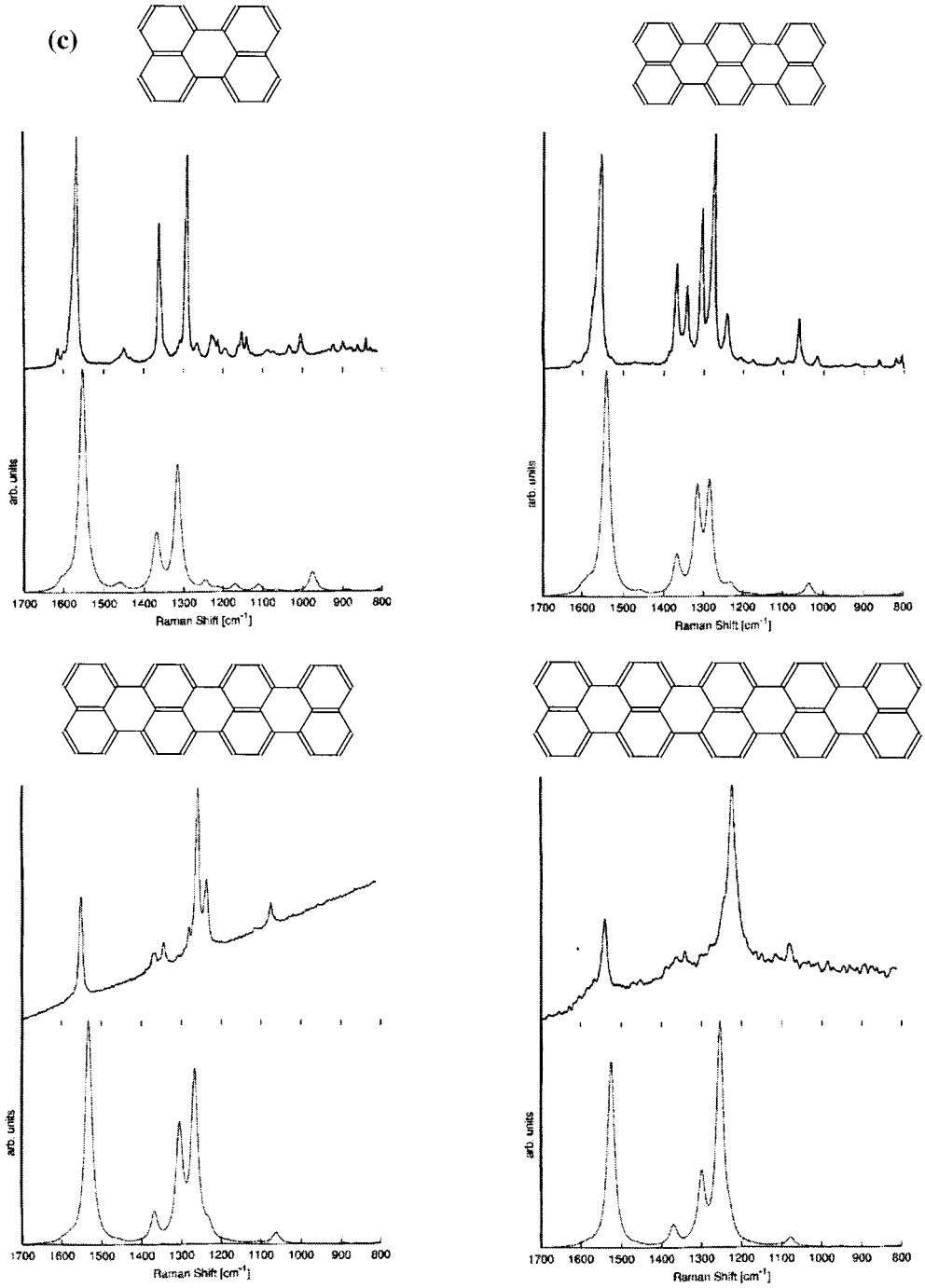

Figure 4. (Continued)

absolute values of α', reported in Figures 3c and 3d, increase while passing from smaller to larger molecules. This fact suggests that the polarizability change associated with a given CC stretching is not just a "local" phenomenon, but involves the delocalized π system as a whole: indeed, the increase of the number of conjugated π electrons available results in a relevant increase of the value of the stretching tensors. This fact justifies point (i). (4) A close inspection of Figures 3c and 3d shows a peculiar trend of the α' values while passing from bond to bond. Following the bond numbering indicated in Figure 2, and by comparison with Figures 3a and 3b, one can realize that the magnitude and sign of α' changes according to the different character of the CC bond (in general, the shorter bonds have positive value of α'). In the case of all-benzenoid molecules (see for instance C114) we can group the CC bonds into two different sets with positive and negative values of α', respectively. In the two sets we find bonds involved in the aromatic sextets (positive α') and bonds linking the aromatic rings (negative α'). C54 follows the same rule, due to its partially benzenoid character. In the case of remarkably non-benzenoid PAHs (such as C84 and C96) we find the opposite trend for α', while following the same bond sequence: a very small, positive value for the inner ring (bond 1), a very large positive value for bond 2, a vanishing α' for bond 3, an so on. This pattern also can be related to the existence of two different sets of CC bonds with a different electrical behavior.

The results commented on in (4) above are noteworthy since they indicate that the electronic structure of all the PAHs considered is very far from the one expected in the case of a perfect, infinite graphene sheet. In this last case, because of

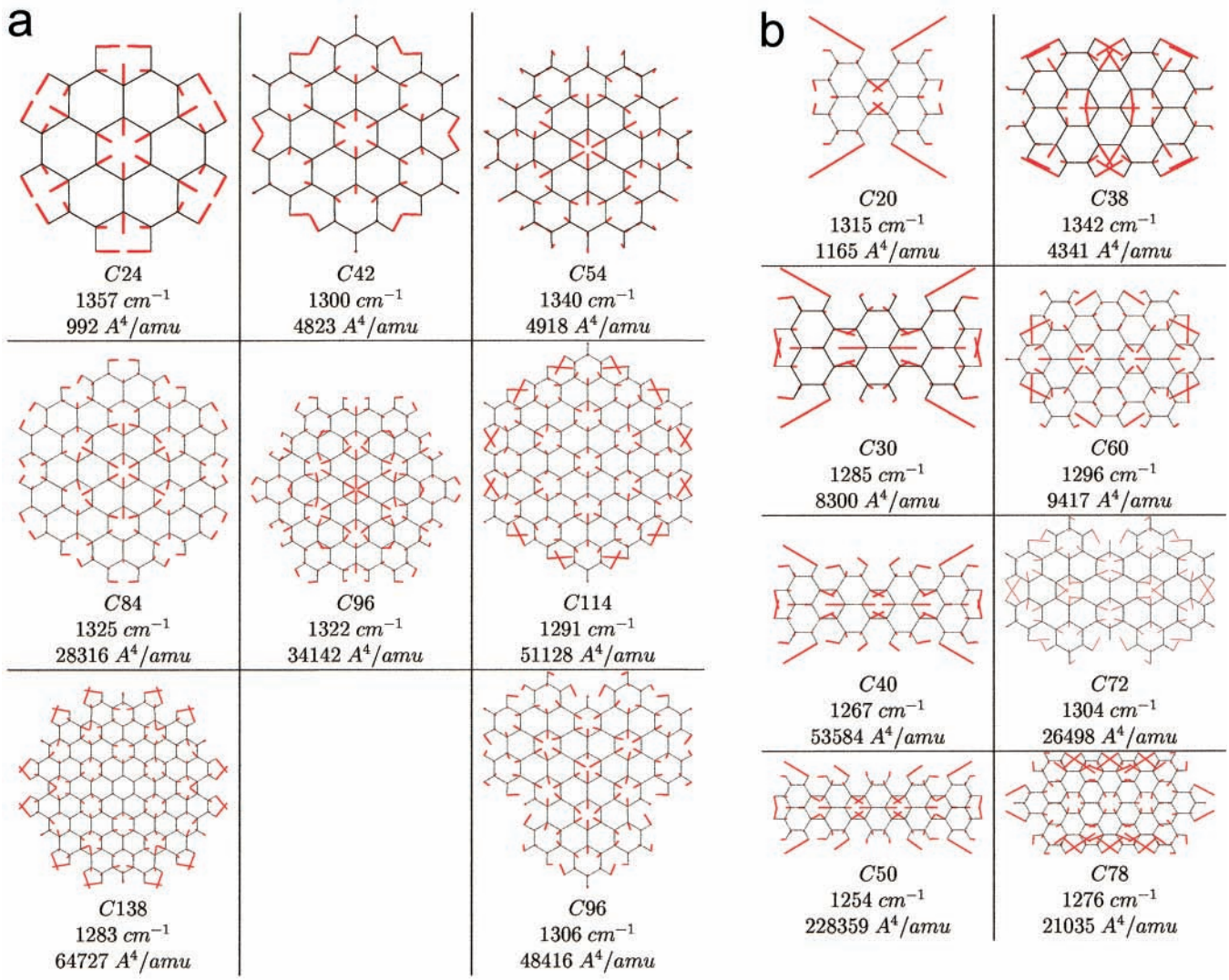

Figure 5. Molecular motions associated with the strongest Raman active normal modes calculated with BLYP/6-31G for (a) D_{6h} and D_{3h} PAHs; (b) D_{2h} PAHs.

symmetry, the values of the α′ tensors, relative to any CC bond, must be identical. One can conclude that the confinement of the conjugated electrons (owing to the finite size of the molecules) dramatically changes the bond property as it is shown by the polarizability derivatives. This peculiarity is certainly reflected by the BLYP/6-31G optimized molecular geometries, which indeed correlate well with α′ parameters. However the differences among the CC bonds are remarkably enhanced when one considers the parameters α′ (opposite sign of α′ for the two different classes of bonds, see section 3.1). Furthermore, as discussed in section 3.1, a marked equalization of bond lengths is computed at the center of the PAH as the molecular size increases. Conversely, the magnitude of the electrical property α′ at the center of the molecule increases with the PAH size. As a result, if one considers the α′ parameters, the different nature of the two classes of CC bonds seems to be amplified as the molecular size increases.

A second consequence directly originating from the behavior of α′ parameters is the fact that vibrations with a large $\mathcal{A}$ character are very strongly Raman active for all the molecules considered. Let us consider a collective vibrational coordinate $\mathcal{A}$, confined in a molecular domain (ideal coordinate $\mathcal{A}$). This coordinate can be described analytically starting from the totally symmetric phonon of graphite at *K* point (see, for instance, refs 11 and 14 for the details). When it is applied to benzenoid PAHs the ideal $\mathcal{A}$ coordinate describes a collective breathing motion of the aromatic sextets (all the rings breathe in phase). As already previously concluded by inspection of the eigenmodes (see section 3.2), we learn that the strong features observed near 1300 cm^{-1} for all the PAHs are due to normal vibrations with a large projection on the ideal $\mathcal{A}$ coordinate.

We discuss now the mechanism leading to the very large polarizability changes associated with deformations along the $\mathcal{A}$ coordinate. This can be done in terms of contributions from local stretching parameters. For a molecule belonging to the D_{6h} point group it is possible to write a general expression for the tensor $\partial\alpha/\partial\mathcal{A}$ in terms of local stretching tensors (referred to the local bond Cartesian reference system, as described in Table 5):

$$\frac{\partial\alpha}{\partial\mathcal{A}} = \sum_i \frac{N_i}{K_i} \begin{pmatrix} \partial\alpha^{xx}/\partial R^i + \partial\alpha^{yy}/\partial R^i & 0 & 0 \\ 0 & \partial\alpha^{xx}/\partial R^i + \partial\alpha^{yy}/\partial R^i & 0 \\ 0 & 0 & 2\partial\alpha^{zz}/\partial R^i \end{pmatrix} \quad (2)$$

In this expression the sum is extended over all the sets of

TABLE 5: Values of CC Stretching Polarizability Tensors (bohr^2) for Selected Bond Stretching of Some PAHs: CC Bonds Are Labeled According to Figure 2 (C114, C78)

C114: CC Bond #1

	x	y	z
x	54.71	0	0
y	0	40.88	0
z	0	0	0.51

C114: CC Bond #2

	x	y	z
x	−36.81	0	0
y	0	−55.24	0
z	0	0	0.50

C78: CC Bond #1

	x	y	z
x	94.82	−13.41	0
y	−13.41	16.00	0
z	0	0	0.51

C78: CC Bond #2

	x	y	z
x	−128.00	0	0
y	0	−7.08	0
z	0	0	0.48

pentarylene: CC Bond #1[a]

	x	y	z
x	−256.45	0	0
y	0	8.94	0
z	0	0	0.36

pentarylene: CC Bond #2[a]

	x	y	z
x	314.63	−20.69	0
y	−20.69	7.96	0
z	0	0	0.46

[a] Bond labels for pentarylene are reported in the sketch below.

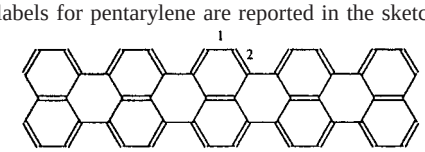

symmetry equivalent CC bonds, N_i is the number of CC bonds in the given *i*th set; $K_i = 4$ if the *i*th set contains bonds belonging to the rings which breathe during $\mathcal{A}$, otherwise $K_i = -2$.

The inspection of the shape of the stretching tensors calculated for the PAHs under study (see, for instance, Table 5) shows that $\partial\alpha^{xx}/R_i + \partial\alpha^{yy}/R_i \approx 3\alpha_i'$, since $\partial\alpha^{zz}/R_i$ is negligibly small with respect to the other tensor elements. Thus we can write eq 2 in a more compact form:

$$\frac{\partial\alpha}{\partial\mathcal{A}} \approx 3\sum_i \frac{N_i}{K_i}\begin{pmatrix}\alpha_i' & 0 & 0\\ 0 & \alpha_i' & 0\\ 0 & 0 & 0\end{pmatrix} \qquad (3)$$

If we now turn back to the conclusions drawn from the analysis of Figure 3c and 3d with regard to the sign and the magnitude of the α' invariant, we can make the following statements. (i) For all-benzenoid systems and for partially benzenoid PAHs, such as C54 and C138, positive α_i' values enter eq 3 with a positive K_i coefficient and negative α_i' values enter eq 3 with a negative K_i coefficient, thus building up, in a cooperative way, a large polarizability change during the $\mathcal{A}$ vibration. (ii) For markedly non-benzenoid systems, such as C84 and C96, all the positive and large α_i' enter with a negative K_i coefficient, giving rise to a cooperative negative change of the molecular polarizability. Small α_i' (positive or negative), all belonging to the rings that breathe during $\mathcal{A}$ (positive K_i) give a negligible contribution to $\partial\alpha/\partial\mathcal{A}$.

A similar reasoning applied to D_{2h} PAHs allows to explain in a parallel way the large Raman activity in the D spectral region (1300 cm^{-1}) also observed for these molecules. More important, the conclusions above also allow to understand the activation of the D line in disordered graphitic materials. Indeed, if we transfer the information so far collected from the quantum-chemical calculations on PAHs, to the graphitic clusters (e.g., those embedded in amorphous carbon materials), we expect that also in confined (finite size) graphitic domains some kind of structural relaxation will lead to the formation of aromatic sextets. If this happens, we expect to find, also in these clusters, two families of CC bonds with markedly different α' values. Making use of this concept and following a very simple symmetry-based reasoning, it can be shown that the immediate consequence of this "dimerization" of the graphite lattice is the Raman activation, in the graphitic domains, of a totally symmetric *K* phonon of graphite.[14] This phonon has exactly the shape of the $\mathcal{A}$ vibration.

3.4. Toward Molecularly Defined Subunits of Graphite. As anticipated above, the ultimate scope of these quantum-chemical computations on PAHs is the interpretation of the spectroscopic behavior of nanosized graphitic clusters such as, for example, those whose existence is claimed in annealed amorphous carbon.[7c] To make the comparison with those experiments more realistic, we need to simulate the effect of confinement produced by the matrix at the edges of the graphitic molecule. One simple way to mimic this effect is to employ a "united-atom" approach (well know in the field of molecular mechanics) and substitute the hydrogen atoms bonded at the edges of the PAHs with a substituent "sub" that we represent with a single atom having a large mass m_{sub}. Such large mass ideally includes the effect of the carbon atoms surrounding the graphitic cluster. If we concentrate on the vibrational frequencies of this model of graphitic island (i.e., the substituted PAH), the effect of the heavy substituents is to decouple the stretching vibrations of the carbon atoms in the PAH from the wagging vibrations of the hydrogens, since the latter have been replaced by heavy substituents. We thus simulate the effect of embedding a PAH molecule into a somewhat rigid matrix, characterized by lower vibrational frequencies. The results for the largest of the PAHs considered, C138, are shown in Figure 6. The simulated Raman spectra for $m_H = 1$ amu and for $m_{sub} = 100$ amu are reported along with the vibrational eigenvectors associated with the strongest peaks near 1300 cm^{-1} (D spectral region). The effect of having large masses on the edges of C138 is remarkable, both on the eigenvectors and on the Raman spectrum. According to the results shown in Figure 6, after the substitution of the hydrogen masses with $m_{sub} = 100$ amu we observe a simplification of the spectrum in the D region. The two strong lines showing up in the spectrum of C138 ($m_H = 1$ amu) are replaced by just one line for $m_{Sub} = 100$ *amu*. Inspection of the eigenvectors corresponding to the intense peaks in the D spectral region discloses the reason for the computed behavior. The eigenvectors in the top panels of Figure 6 correspond to the two strongest computed Raman bands and, according to the discussions in previous sections, they are dominated by a large contribution from the ideal $\mathcal{A}$ ring-breathing coordinate. However, owing to the coupling with CH wagging vibrations, they also contain a relevant contribution

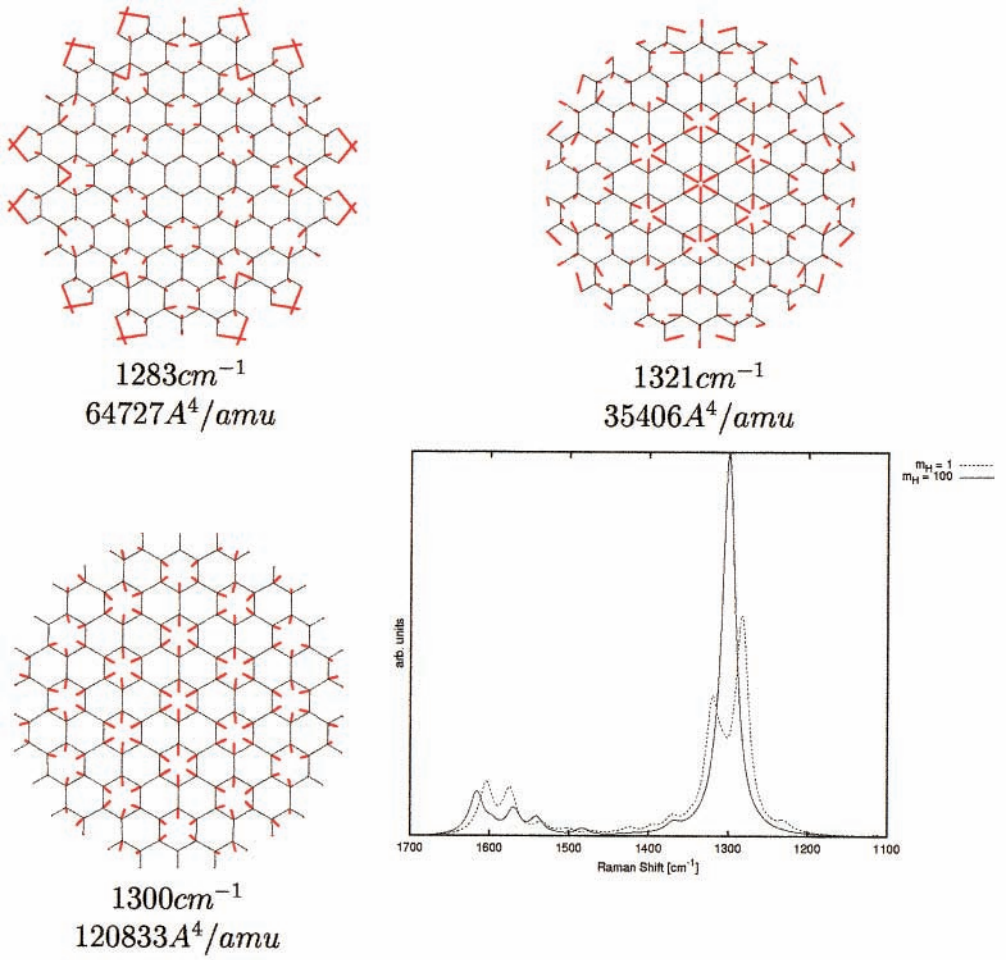

Figure 6. Effect of the change of masses ($m_H = 1 \rightarrow m_H = 100$) on the shape and frequency of the strongest Raman vibrations of C138 in the 1300 cm^{-1} region. The effect on the calculated Raman spectrum is also shown.

from these local motions. For the vibration at 1321 cm^{-1}, the $\mathcal{A}$ contribution is more localized in the inner rings of the molecule, whereas for the vibration at 1283 cm^{-1} the $\mathcal{A}$ contribution is located on the periphery of the molecule. The coupling with CH waggings is always present, since the typical frequencies of CH wagging vibrations lie in the spectral region of the D band.[25] When we consider the case with $m_{sub} = 100$ amu, the characteristic frequencies for the C-sub waggings are remarkably lowered ($\nu_{wag} \approx 100$ cm^{-1} in the case of C138), whereas the frequency of the $\mathcal{A}$ vibration is practically unaffected. Thus we find a unique strong Raman line at 1300 cm^{-1} (Figure 6), which overlaps almost completely with the ideal collective $\mathcal{A}$ vibration, that is, it is spread out uniformly over all the rings of the molecule (see lower left panel of Figure 6).

A similar behavior for the vibrations in the D-band region is computed for all the other PAHs studied (see Table 6). Generally speaking, for the "real" molecules ($m_H = 1$ amu) a few (two or three) strong Raman bands are predicted in the region of the D band, owing to the coupling of the ideal $\mathcal{A}$ vibration with CH wagging motions. For the models of graphitic islands ($m_{sub} = 100$ amu) these features originate a unique band, with an intensity approximately equal to the sum of the intensities of the original lines. This observation is a nice and independent proof of the fact that the Raman activity of PAHs in the region near 1300 cm^{-1} is due to the large polarizability change associated with the collective breathing vibration $\mathcal{A}$, and is not related to the coupling with CH waggings. We can then safely state that in amorphous pure carbon, large Raman activity of the D line is expected when graphitic domains develop, i.e., during annealing.[7c] Furthermore, the simplification of the computed Raman spectrum for the models of graphitic islands, compared to PAHs, is in agreement with the experimental spectra of carbonaceous materials,[7] in which the D band is rather narrow and shows little evidence of substructure. Finally, the

TABLE 6: Substitution of Hydrogen with a Large Mass Group Substituent in the "United-Atom" Representation ($m_H = 1 \rightarrow m_{sub} = 100$)[a]

	$m_{sub} = 100$		$m_H = 1$	
PAH	ν	I_R	ν	I_R
C24	1343	1023	1357	992
C42	1318	5321	1299	4823
			1347	642
C54	1319	8894	1286	3075
			1340	4918
C84	1320	31566	1253	1890
			1325	28316
			1371	1668
C96	1322	33801	1232	3476
			1322	34142
C114	1307	72166	1291	51128
			1312	23775
C138	1300	120833	1283	64727
			1307	10793
			1321	35406

[a] Effect on the vibrational frequencies (cm^{-1}) and Raman intensities I_R (Å^4/amu) of the strongest A_{1g} modes (D-band region) of the D_{6h} PAHs.

calculations demonstrate that the possible content of hydrogen is irrelevant for the intensity of the D band.

4. Conclusions

We have investigated the ground-state structure, vibrational frequencies, and Raman intensities of several polycyclic aromatic hydrocarbons with the help of density functional theory calculations. Several PAHs characterized by different size and shape have been considered in order to explore the effect on Raman spectra and their associated electric properties.

The computed Raman spectra are in good agreement with the experimental data, and it is found that the largest computed intensities correspond to vibrations with a large content of ideal coordinates $\mathcal{A}$ and Я. The simplification of the Raman spectra expected for graphitic islands of molecular size (compared to the spectra of PAHs) is also modeled by substituting the hydrogens of PAHs with heavy groups, according to a united-atom approach.

The analysis in terms of local contributions to Raman intensities clarifies the origin of the large Raman cross section for the few bands at about 1300 cm^{-1}, observed for all the PAHs examined. On the same basis, the origin of the D line induced in disordered graphitic materials is rationalized. It is shown that the values of the local stretching polarizability tensors (α' parameters) can be used as a very sensitive probe of the character of CC bonds in PAH molecules. More specifically, they allow to easily identify the presence of aromatic sextets in all-benzenoid PAHs. Moreover, the α' correlate with the equilibrium bond lengths that result from quantum-chemical calculations of equilibrium structure. The analysis of both electrical (α') and structural (bond lengths) parameters for the PAHs studied in this work suggests a classification of the PAHs in two groups related more to their "benzenoid" character than to the shape of their periphery.

Acknowledgment. We are deeply indebted to Prof. K. Müllen (Max Planck Institut für Polymerforschung) who has provided us with the samples of structurally defined PAHs studied in this work. The availability of these materials has opened new horizons to our work. Fundings from CNR, "Nanotechnologies", and "Progetto finalizzato materiali speciali per tecnologie avanzate: Thin layers molecular materials for electronics and nonlinear optics", are gratefully acknowledged. This research has been supported by the University of Bologna (Funds for selected research topics: Project "Materiali innovativi"), by CNR (Project "Applicazioni di spettroscopie ottiche" and "Progetto finalizzato materiali speciali per tecnologie avanzate II"), and from MURST (Project "Analisi della struttura vibrazionale di spettri elettronici", ex 60 %, Project "Supramolecular devices", ex 40 %).

References and Notes

(1) Clar, E. *The aromatic sextet*, Wiley: London, 1972.

(2) Barone, P. M. V. B.; Camilo, A., Jr.; Galvao, D. S. *Phys. Rev. Lett.* **1996**, *77*, 1186.

(3) Schlemmer, S.; Cook, D. J.; Harrison, J. A.; Wurfel, B.; Chapman, W.; Saykally, R. J. *Science* **1994**, *265*, 1686. Cook, D. J.; Schlemmer, S.; Balucani, N.; Wagner, D. R.; Steiner, B.; Saykally, R. J. *Nature* **1996**, *380*, 227. Allamandola, L. J.; Tielens, A. G. G. M.; Barker, J. R. *Astrophys. J. Suppl. Ser.* **1989**, *71*, 733. Hudgins, D. M.; Bauschlicher C. W., Jr.; Allamandola, L. J. *Spectrochim. Acta A* **2001**, *57*, 907.

(4) Ito, S.; Wehmeier, M.; Brand, J. D.; Kübel, C.; Epsch, R.; Rabe, J. P.; Müllen, K. *Chem. Eur. J.* **2000**, *6*, 4327. Boden, N.; Bushby, R. J.; Clements, J. *J. Chem. Phys.* **1993**, *98*, 5920. Markovitsi, D.; Lecuyer, I.; Lianos, P.; Malthete, J. *J. Chem. Soc., Faraday Trans.* **1991**, *87*, 1785.

(5) Harvey, R. G. *Polycyclic Aromatic Hydrocarbons*; Wiley-VCH: New York, 1997.

(6) Watson, M. D.; Fechtenkötter, A.; Müllen, K. *Chem. Rev.* **2001**, *101*, 1267. Stabel, A.; Herwig, P.; Müllen, K.; Rabe, J. P. *Angew. Chem., Int. Ed. Engl.* **1995**, *34*, 1609. Fechtenkötter, A.; Saalwächter, K.; Harbison, M. A.; Müllen, K.; Spiess, H. W. *Angew. Chem., Int. Ed. Engl.* **1999**, *38*, 3039.

(7) (a) Dresselhaus, M. S.; Dresselhaus, G.; Eklund, P. C. *Science of Fullerenes and Carbon Nanotubes*; Academic Press: San Diego, 1996. (b) Riedo, E.; Magnano, E.; Rubini, S.; Sancrotti, M.; Barborini, E.; Piseri, P.; Milani, P. *Solid State Commun.* **2000**, *116*, 287. (c) Ferrari, A. C.; Robertson, J. *Phys. Rev. B* **2000**, *61*, 1. (d) Nemanich, R. J.; Solin, S. A. *Phys. Rev. B* **1979**, *20*, 392. (e) Tuistra, F.; Koenig, J. L. *J. Chem. Phys.* **1970**, *53*, 1126. (f) Kawashima, Y.; Katagiri, G.; *Phys. Rev. B* **1995**, *52*, 10053.

(8) Pócsik, I.; Hundhausen, M.; Koós, M.; Ley, L. *J. Non-Cryst. Solids* **1998**, *227*−*230*, 1083.

(9) Tan, P. H.; Deng, Y. M.; Zhao, Q. *Phys. Rev. B* **1998**, *58*, 5435.

(10) Mapelli, C.; Castiglioni, C.; Meroni, E.; Zerbi, G. *J. Mol. Struct.* **1999**, *480*−*481*, 615.

(11) Mapelli, C.; Castiglioni, C.; Zerbi, G.; Müllen, K. *Phys. Rev. B* **1999**, *60*, 12710.

(12) Castiglioni, C.; Mapelli, C.; Negri, F.; Zerbi, G. *J. Chem. Phys.* **2001**, *114*, 963.

(13) Rigolio, M.; Castiglioni, C.; Zerbi, G.; Negri, F. *J. Mol. Struct.* **2001**, *563*−*564*, 79.

(14) Castiglioni, C.; Negri, F.; Rigolio, M.; Zerbi, G. *J. Chem. Phys.* **2001**, *115*, 3769.

(15) Ohno, K. *J. Chem. Phys.* **1991**, *95*, 5524.

(16) Becke, A. D. *Phys. Rev. A* **1998**, *38*, 3098.

(17) Lee, C.; Yang, W.; Parr, R. G. *Phys. Rev. B* **1988**, *37*, 785.

(18) Gaussian 98, Revision A.3, Frisch, M. J.; Trucks, G. W.; Schlegel, H. B.; Scuseria, G. E.; Robb, M. A.; Cheeseman, J. R.; Zakrzewski, V. G.; Montgomery, J. A., Jr.; Stratmann, R. E.; Burant, J. C.; Dapprich, S.; Millam, J. M.; Daniels, A. D.; Kudin, K. N.; Strain, M. C.; Farkas, O.; Tomasi, J.; Barone, V.; Cossi, M.; Cammi, R.; Mennucci, B.; Pomelli, C.; Adamo, C.; Clifford, S.; Ochterski, J.; Petersson, G. A.; Ayala, P. Y.; Cui, Q.; Morokuma, K.; Malick, D. K.; Rabuck, A. D.; Raghavachari, K.; Foresman, J. B.; Cioslowski, J.; Ortiz, J. V.; Stefanov, B. B.; Liu, G.; Liashenko, A.; Piskorz, P.; Komaromi, I.; Gomperts, R.; Martin, R. L.; Fox, D. J.; Keith, T.; Al-Laham, M. A.; Peng, C. Y.; Nanayakkara, A.; Gonzalez, C.; Challacombe, M.; Gill, P. M. W.; Johnson, B.; Chen, W.; Wong, M. W.; Andres, J. L.; Gonzalez, C.; Head-Gordon, M.; Replogle, E. S.; Pople, J. A. Gaussian, Inc.: Pittsburgh, PA, 1998.

(19) Rigolio, M. *Thesis in Chemical Engineering*, Politecnico di Milano: Milano, 2000.

(20) Stein, S. E.; Brown, R. J.; *J. Am. Chem. Soc.* **1987**, *109*, 3721.

(21) Armit, J. W.; Robinson, R.; *J. Chem. Soc.* **1925**, 1604.

(22) Rumi, C.; Zerbi, G.; Müllen, K.; Rehahn, M. *J. Chem. Phys.* **1997**, *106*, 24.

(23) Fleischer, U.; Pulay, P. *J. Raman Spectrosc.* **1998**, *29*, 473.

(24) Fleischer, U.; Pulay, P. Babkov, L. M.; Glyadkovskii, V. I.; Davydova, N. I.; Karpova, V. A.; Klimova, L. A.; Kovner, M. A.; Suchinskii, M. M.; Terekhov, A. A.; Shpolskii, E. V. *Opt. Spektrosc.* **1973**, *34*, 38.

(25) Colthup, N. B.; Daly, L. H.; Wiberley, S. E. *Introduction to Infrared and Raman Spectroscopy*; Academic Press: New York, 1975.